

Received June 18, 2020, accepted June 25, 2020, date of publication June 30, 2020, date of current version July 20, 2020.

Digital Object Identifier 10.1109/ACCESS.2020.3005981

Anti-Motion Interference Wearable Device for Monitoring Blood Oxygen Saturation Based on Sliding Window Algorithm

BIN JIAO 

School of Art and Design, Zhengzhou University of Aeronautics, Zhengzhou 450000, China

e-mail: jiaobin@zua.edu.cn

This work was supported by the Henan Center for Outstanding Overseas Scientists: Foreign Expert Center of Design Teaching System of Florence Academy of Fine Arts under Grant GZS2020009.


ABSTRACT Wearable multi-physiological parameter monitoring technology can realize non-intrusive, non-invasive daily health monitoring of the human body. It has the characteristics of convenient operation, long-term continuous work, display of results, abnormal physiological condition alarm and wireless data transmission. First, an improved sliding window confidence propagation algorithm is proposed, which reduces the inefficient iterative process in the decoding process by correlation coefficients and reduces the running time of the algorithm by more than 1.5 times; designing a channel noise estimation method based on sliding window confidence propagation algorithm, and The source coding is similar. In order to estimate the local statistical parameters of the channel noise, the confidence propagation, the decoder uses the local partial probability of the adjacent accompanying child nodes to estimate the noise parameters of the channel noise. Secondly, the design and research of the blood oxygen saturation monitor, including filtering out high-frequency glitch noise, low-frequency baseline drift noise, and mixing and sudden motion interference noise, also achieved rapid and accurate extraction of pulse wave feature points, and calculated the blood oxygen value and pulse rate value. Compared with the traditional oximeter, the filtering algorithm and pulse wave feature point extraction algorithm on the oximeter software have less calculation amount and higher real-time performance. Finally, the relevant test experiment of the blood oxygen saturation monitor proves that the blood oximeter has good stability, accuracy and sensitivity. The practical use of anti-motion interference wearable devices not only shows that the wearable PPG sensor in this paper can stably obtain high-quality PPG signals, but also reflects its many applications in the field of real-time blood.

INDEX TERMS Sliding window algorithm, blood oxygen saturation, anti-motion interference, wearable.

I. INTRODUCTION

Blood oxygen saturation characterizes the oxygen content of the human blood, can effectively reflect the physiological state of the human circulatory system and respiratory system, and plays an active role in the diagnosis and health monitoring [1]. Nowadays, non-invasive blood oxygen detection methods have been well developed, from traditional transmission detection methods to reflective blood oxygen detection [2], portable blood oxygen detection and blood oxygen detection equipment with integrated wireless module [3]. However, due to the influence of factors such as structure,

power consumption and motion interference, its application in a dynamic environment is limited, so that the blood oxygen saturation detection still cannot accurately obtain the blood oxygen state of the human body in real time. The physiological signal of the human body in a natural state can more accurately reflect its physiological state, especially in some special occasions, such as post-operative follow-up observation, community medical care and family health care, all need to be real-time without affecting people's daily work and life. Obtain blood oxygen saturation information [4], [5]; another example is the soldiers in the battlefield environment, which can obtain their blood oxygen saturation status in real time, which can effectively and timely determine whether the soldiers have tension pneumothorax or suffocation caused by

The associate editor coordinating the review of this manuscript and approving it for publication was Wei Wei .

war trauma. The occurrence of the situation makes it easy to take rescue measures as soon as possible to save lives.

In order to achieve dynamic real-time monitoring of blood oxygen saturation, the following three requirements need to be met: a physical structure suitable for wearing, a low-power design that can monitor for a longer period of time, and a better motion interference cancellation scheme. In recent years, there have been some studies on wireless detection methods of blood oxygen saturation, but most of them only focus on the design of wireless modules, and no specific method for eliminating motion interference in wireless portable monitoring is proposed [6], [7]. With the continuous development of wireless communication networks in recent years, distributed coding technology has regained attention and development. Literature [8] first proposed the idea of using LDPC codes to construct lossless distributed coding to make it have better performance. At present, this method has been widely used in source coding and channel coding systems. For non-stationary sources, it is often difficult for decoders to obtain accurate probability distributions of related sources. A relatively common practice is to use the average estimate of related sources to replace the accurate values of related parameters [9], [10], which is equivalent to treating non-stationary sources as stationary sources, so there will be more in the compression and decoding process Large bit rate loss. At present, the solution to this problem is to estimate relevant unknown parameters while decoding, which is mainly divided into distributed source parameter estimation and channel parameter estimation. Consider the asymmetric coding communication model based on side information as two different virtual channels. The first one is the virtual channel between the side information and the source. The crossover probability between them is considered to be caused by the virtual channel noise. [11], [12], the second is that the channel is the actual communication channel, and then the idea of using channel codes to realize joint source channel coding is proposed. Literature [13], [14] proposed to use adaptive Bayesian method to estimate the channel noise variance in the asynchronous communication model, effectively solving the problem of unknown noise distribution parameters in noisy channels. However, the above studies all assume that the channel noise statistical characteristics are constant, that is, stable. In practice, however, the statistical characteristics of channel noise often change continuously over time. In order to solve the noise estimation problem of non-stationary channels, the literature [15], [16] proposed a particle confidence propagation algorithm, which introduces a particle filtering process in the LDPC code's confidence propagation iteration to achieve accurate estimation of the statistical characteristics of non-stationary channel noise. Mainly including two stages of particle filtering and confidence propagation. In the particle filtering stage, random samples with weights are randomly sampled [17], [18] to estimate the noise changes in the code word bits. The particles with equal weights are given to each

variable node at the initial moment. As the iteration of the confidence propagation continues, the weights are discarded Small particles are particles with low confidence. Finally, for the particles that are retained, the posterior probability algorithm is used to estimate the noise parameters [19], [20]. First, use this estimator to accurately estimate the statistical characteristics of non-stationary sources, and then run a standard confidence propagation algorithm to decode [21], [22]. Subsequently, it is proposed to use a two-level estimator to optimize the maximum likelihood estimator, that is, to introduce expectation maximization. This method is then extended to the application of non-stationary binary channel noise estimation. Due to the high complexity of the particle filtering algorithm, the literature [23], [24] proposes a non-stationary source local parameter estimation algorithm based on expected propagation. At present, the technology development of the blood oxygen saturation monitor is relatively mature, and its overall trend is to miniaturize, that is, the collection, processing and display are integrated [25], [26], but the current blood oxygen saturation monitor still has many disadvantages, such as high cost, Large power consumption, poor real-time performance, low measurement accuracy, poor stability, and need to be further intelligent and networked [27]. Another research content based on pulse wave blood oxygen saturation measurement is the filtering of noise signals of various frequencies in the pulse wave signal. First, the filtering methods of pulse wave high-frequency noise are as follows: for example, literature [28] proposes to use empirical mode decomposition method based on continuous mean square error criterion to eliminate high-frequency noise in pulse wave signal [29]; References [30], [31] propose to eliminate high-frequency noise in pulse wave signals; the above method first requires empirical mode decomposition of the pulse wave signal, then removes the intrinsic mode components of high-frequency noise, and finally reconstructs the signal [32], [33] Obviously, it takes a lot of CPU time in practice, and the real-time performance of the system will not be guaranteed. The physiological parameters detected by the second type of wearable monitoring equipment are more abundant than those of the first generation, and the implemented form presents a concentrated feature, mainly including wearable clothing [34]. In addition, intelligent equipment including mattresses [35] and stools [36] has also been developed to detect physiological parameters including blood pressure, heart rate, breathing rate and body temperature. The third type of wearable monitoring device (flexible electronic device) is quite different from the first two types. With the development of materials science and semiconductor technology, it has the characteristics of miniaturization and flexibility, mainly including epidermal electronic equipment [37], Electronic skin [38], etc. At present, this type of wearable monitoring device is still in the research stage.

This article introduces the basic concepts, classification, coding principles and decoding principles of low-density

parity-check codes; introduces probabilistic decoding algorithms and standard confidence propagation algorithms; introduces sliding window confidence propagation algorithms, analyzes their problems, and gives optimization solutions, That is, an improved sliding window confidence propagation algorithm. A joint source channel coding based on sliding window confidence propagation is proposed. By analyzing the experimental results of two different LDPC codes, the specific reasons that affect the decoding performance are given. In response to these three requirements, the design and discussion of wearable blood oxygen saturation monitoring methods have achieved good results in terms of miniaturization, low power consumption and resistance to sports interference.

II. SLIDING WINDOW CONFIDENCE PROPAGATION ALGORITHM AND ITS IMPROVEMENT

A. SLIDING WINDOW CONFIDENCE PROPAGATION ALGORITHM

After receiving the companion s , the decoder runs the confidence propagation algorithm to restore x . For the convenience of description, LDPC codes are often expressed using bipartite graphs. The bipartite graph generally contains two kinds of nodes: variable node x and check node s . The edge used for the connection between the variable node and the check node. To facilitate the description of the basic principles of the confidence propagation algorithm, Table 1 defines the relevant symbols to be used.

TABLE 1. Symbol definition of confidence propagation algorithm.

Symbol	Meaning
\hat{q}_i	Estimated value of q_i
\hat{y}_i	Estimated value of y_i
η_{ij}	Confidence that the variable node y_i passes to the check node t_i
κ_{ij}	Confidence that the variable node t_i passes to the check node y_i
λ_i^0	Variable node y_i own confidence
λ_i	Variable node y_i own total confidence

Before running the confidence propagation algorithm, the decoder needs to initialize the variable nodes. In general, the local partial probability of the source cannot be known at the decoding end, and the global partial probability is relatively easy to obtain, so the global partial probability can be used as an alternative, and then the decoder iteratively runs the following four steps:

(1) First calculate the message passed by the variable node to the check node.

$$\frac{1 - \eta_{ij}}{\eta_{ij}} = \frac{1 - \lambda_i}{\lambda_i} / \frac{1 - \kappa_{ij}}{\kappa_{ij}} \quad (1)$$

(2) Then calculate the message passed by the check node to the variable node.

$$1 - 2\kappa_{ij} = \prod_i 1 - 2\eta_{ij} \quad (2)$$

(3) Next, calculate the total confidence

$$\frac{1 - \lambda_i}{\lambda_i} = \frac{1 - \lambda_i^0}{\lambda_i^0} \prod_j \frac{1 - \kappa_{ij}}{\kappa_{ij}} \quad (3)$$

(4) Finally, make a hard decision on node x

$$\hat{y}_i = \begin{cases} 0, & \lambda_i < 0.5 \\ 1, & \lambda_i \geq 0.5 \end{cases} \quad (4)$$

The algorithm dynamically estimates the local partial probability of non-stationary binary sources while decoding, thereby improving the source compression performance. The sliding window confidence propagation algorithm introduces two steps: sliding window setting and parameter estimation based on the standard confidence propagation algorithm. The best neighborhood of each variable node is found, that is, the best window the partial probability of the adjacent source node in the window is used to estimate the partial probability of the current source node, so that the model parameters are more accurate. The process is shown in Figure 1.

B. IMPROVED SLIDING WINDOW CONFIDENCE PROPAGATION ALGORITHM

In the setting of the sliding window size, the sliding window size that makes the current partial probability and the estimated partial probability have the smallest sum of square errors is adopted as the optimal sliding window. However, the experimental results show that for different noise channels, the uniform performance of the sum of squared errors will not achieve the best performance. Therefore, this paper establishes a unified model for different channel noise and uses different loss functions to achieve the best performance.

Let $y_i \in \{0, 1\}$ be the value of the binary source at node y_i , t_i is the message at the receiving end, then:

$$t_i = y_i + \chi_i \quad (5)$$

According to the maximum likelihood estimation, the objective function is:

$$L = \prod_{i=0}^{n-1} \frac{1}{\sqrt{2\tau}} \exp \left(\frac{(t_i - y_i)^2}{2\sigma^2} \right) \quad (6)$$

According to the maximum likelihood estimate, it is equivalent to making the following formula obtain the minimum value:

$$\frac{1}{2} \sum_{i=0}^{n-1} (t_i - y_i)^2 \quad (7)$$

As shown in Figure 2, the best window is determined by using the average of the total confidence of all nodes around the intermediate variable nodes, and treating all the nodes

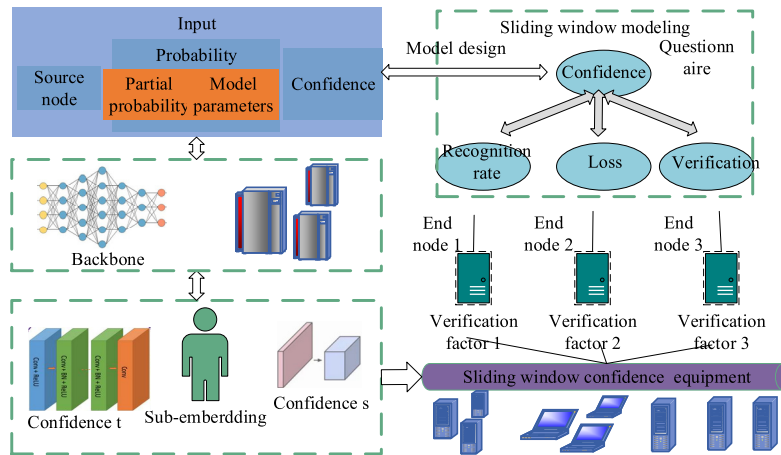


FIGURE 1. Flow of sliding window confidence propagation algorithm.

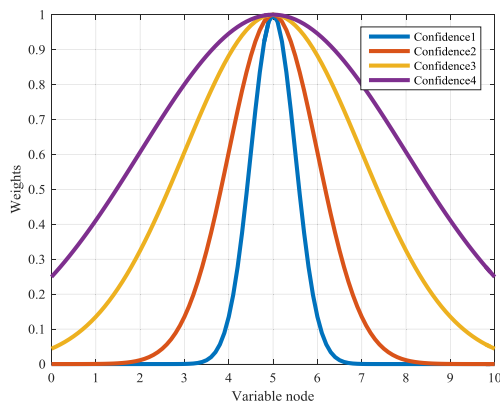


FIGURE 2. Gaussian distribution.

in the window equally. The importance of different nodes in the actual window is different. Therefore, variable nodes with different distances and weights are introduced into the sliding window algorithm improved by this method to give different weights. The distribution of small weights depends on the smaller the distance from the current, the closer the relationship is, and the greater the weight, the smaller the weight.

C. NON-STATIONARY CHANNEL PARAMETER ESTIMATION BASED ON SLIDING WINDOW CONFIDENCE PROPAGATION ALGORITHM

In the joint source channel coding, the transmission channel is generally a noisy channel. Therefore, not only the source parameters need to be estimated, but also the channel statistical parameters need to be estimated in real time. The sliding window confidence propagation algorithm can not only accurately estimate the parameters of non-stationary sources, but also estimate the local statistical parameters of non-stationary channels. Similar to the parameter estimation of binary non-stationary sources, the joint source channel coding process based on the sliding window confidence propagation algorithm is shown in Figure 3. This algorithm is

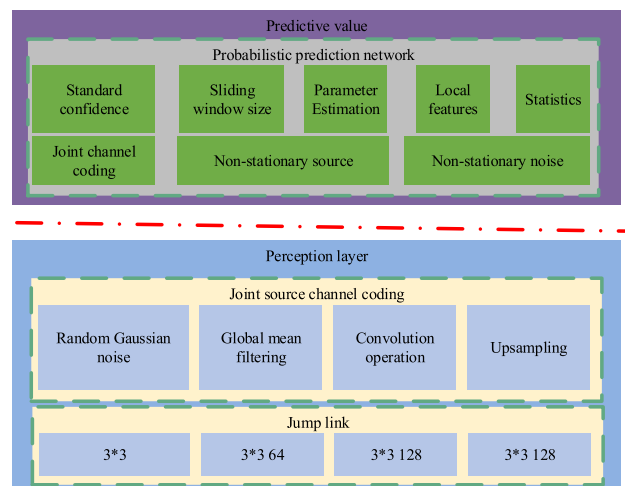


FIGURE 3. Joint source channel coding process based on sliding window algorithm.

also divided into three links: standard confidence propagation, window size selection, and parameters Estimate three links. Different from it, the parameter estimation link needs to estimate not only the estimated partial probability of non-stationary sources but also the local statistical characteristics of non-stationary noise.

III. RESEARCH ON ANTI-MOTION INTERFERENCE WEARABLE DEVICE BASED ON SLIDING WINDOW ALGORITHM FOR BLOOD OXYGEN SATURATION MONITORING

The common filter design has a fixed passband frequency and has limited effect on changing noise. The adaptive filter can make corresponding adjustments as the noise frequency changes, and automatically adjust the current filter parameters according to the filtering results obtained at the previous moment, thereby optimizing the filtering results. The adaptive filter can realize the dynamic adjustment of parameters according to the set optimization criteria, and has the ability of self-learning.

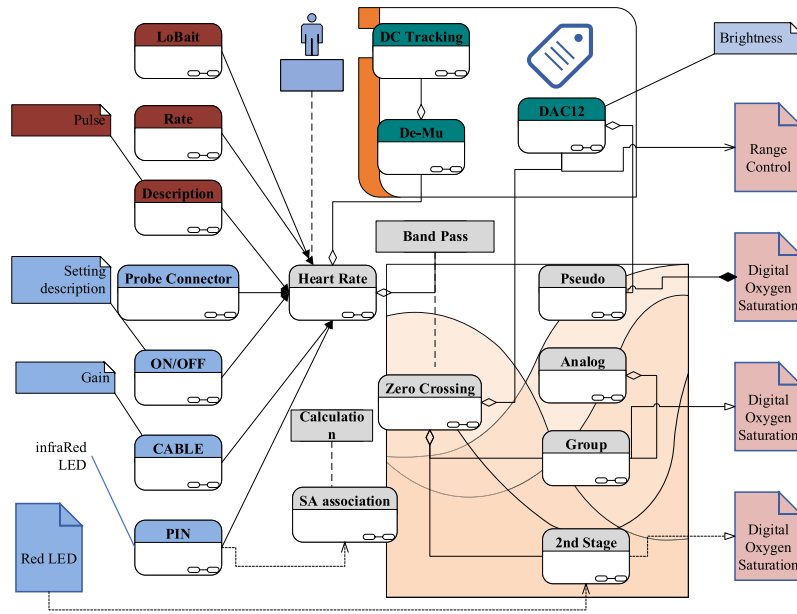


FIGURE 4. Block diagram of the measurement principle of the digital blood oxygen saturation monitor.

Figure 4 is a block diagram of the measurement principle of the digital blood oxygen saturation monitor. It mainly uses digital signal processing to obtain the DC component from the photoelectric volume pulse wave signal, and uses it as the DC bias of the AC amplifier circuit, and then amplifies the AC signal. Compared with the analogue blood oxygen saturation monitor, the number of amplifiers used has been reduced, but because of the need for feedback, it is more difficult to control, and in addition it is also susceptible to low-frequency drift.

Table 2 shows the function of each module, the important problems to be solved and the solutions. Compared with the traditional analogue blood oxygen saturation monitor, it removes the signal amplification and AC-DC separation circuit, which simplifies the hardware circuit, thereby reducing the cost; and compared with the digital blood oxygen saturation monitor, it removes the DC filter and The AC amplifier circuit will adopt a new method to ensure the detection accuracy of the AC component.

A. BLOOD OXYGEN SATURATION MONITORING AND MEASURING PRINCIPLE

Wearable blood oxygen saturation monitoring is intended to collect blood oxygen information without affecting people’s normal activities. The usual transmission blood oxygen detection method can only be placed on the fingers or ears. For the detection of movement status, the probe is not easy to fix and greatly affects people’s daily life, and cannot meet the requirements of dynamic blood oxygen monitoring. The reflective blood oxygen detection method is not limited by the placement of the probe. It can be embedded in the headband and fixed on the forehead of the human body to obtain blood oxygen information in real time.

TABLE 2. Function of each module.

Module	Function
Power management module	The power supply source of the whole system is two No. 7 mercury-free alkaline batteries, whose total voltage is 3V, and the 3V generates 3.3V1 through the DC-DC boost chip to supply power to the MCU microcontroller, key control circuit, LDO chip, and the key control LDO The chip generates 3.3V2 to power the light source driving module, photoelectric receiving module, OLED LCD screen, FBT 06 Bluetooth
MCU microcontroller	Microcontroller KL25, realize IO, LPTMR driving lights, AD acquisition, data processing (rapid filtering method of noise signal of each frequency in pulse wave signal, pulse wave feature point extraction algorithm, calculating blood oxygen value SpO2 and pulse rate value PR) . The OLED LCD screen displays the results and sends data to the PC LABVIEW host computer and mobile phone with Bluetooth Android operating system.
MKL25Z128VLK4	660nm wavelength red LED and 900nm wavelength infrared LED
Common anode light emitting diode	Convert photocurrent signal to voltage signal

After the incident light passes through the human tissue, it is scattered many times, and part of it returns to the surface of the skin, which is reflected in the form of reflected light from a macro perspective. Literature has shown that the distance between the light source and the receiver determines the depth of detectable light incident on human tissue, so choosing different detection distances can obtain blood oxygen information of tissues of different depths. In the design,

the LED and the receiving head are placed at a distance of 1.5 cm to obtain better information about the blood oxygen saturation of the human body.

According to the photon diffusion equation and Lambert's law, the calculation formula of the reflective blood oxygen saturation can be derived:

$$SpO_2 = A_i - B_i \frac{I_{AC}^\lambda}{I_{DC}^\lambda} \quad (8)$$

Among them, I_{AC}^λ , I_{DC}^λ represents the AC component and DC component of the light intensity at the wave length λ , and A and B are the blood oxygen calibration coefficients. It can be seen from the formula that the reflection-type blood oxygen saturation can be calculated by the AC and DC information of the photoelectric volume pulse wave signal as the transmission-type blood oxygen saturation.

The wearable design of blood oxygen saturation monitoring based on sliding window algorithm is:

(1) The hardware design mainly considers the miniaturization and wearability of the instrument. It is composed of four parts: a reflective probe, a signal acquisition module, a light source driver, and wireless transceiver, to realize the functions of light emission, detection and wireless transmission. The entire hardware is embedded in the wearable headband and communicates with the outside world through wireless transceiver.

(2) Reflective probe. Reflective probe contains only two components: dual light source LED and optical frequency conversion receiver head. The LED and the receiving head are fixed to the front side of the headband at a pitch of 1.5 cm, and connected to the control and acquisition hardware module fixed on the side of the headband with short wires. The probe is located on the forehead when worn, and the hardware circuit module is located on the side of the head.

The light source uses 660 nm, 905 nm dual wave length LED, which is only controlled by the positive and negative pins. When the direction of the current flowing through the LED is positive or negative, it can emit red or infrared light. The receiving device uses an optical frequency conversion receiving head, which is a special infrared receiving circuit, which integrates the infrared receiving tube and the amplifying circuit, can sense the light intensity and convert it into a frequency size.

(3) Signal acquisition module. The signal acquisition module mainly completes the task of PPG signal digitization. Most of the designs are implemented with photoelectric receivers, signal conditioning circuits, and AD sampling. This design is a common method to achieve analog signal acquisition, so it is widely used. However, this method of data sampling in wearable oxygen saturation monitoring has some disadvantages: ① The PPG signal obtained by the probe is transmitted to the acquisition module in the form of analog voltage through the wire, and it is easy to introduce interference during the transmission process. ② To calculate the blood oxygen saturation, it is necessary to obtain the PPG signal of two light waves attenuated by human tissue at the

same time. Usually, the pulse modulation method is used to make the light-emitting LED emit light alternately at a certain frequency. In this way, the voltage output by the photocell is not a continuous signal, but a set of pulse sequences, and the PPG signal is loaded in this series of pulse sequences. At this time, analog signal conditioning is performed on this signal. For example, low-pass or high-pass filtering is easy to attenuate the entire signal, and it is not possible to filter out only interfering signals like continuous signal processing. ③ There are many devices required for the sampling circuit, the structure is complex, it is not easy to miniaturize, and it cannot meet the requirements of wearable monitoring.

(4) LED drive circuit. The central processor uses MSP430F1611 to design. This is a 16-bit ultra-low-power single-chip microcomputer, which meets the requirements of low-power design; its internal two integrated D / A digital-to-analog conversion channels can easily control the LED light-emitting state without adding additional the conversion chip simplifies the circuit. The voltage control signal after digital-to-analog conversion is converted into a stable current signal by a constant current source circuit composed of a precision unit differential amplifier INA105 to drive the LED to emit light. By changing the output voltage value of D / A digital-to-analog conversion, the light-emitting state of the LED can be conveniently controlled, and the circuit is simple and easy to miniaturize.

(5) Wireless transceiver module. In the design, the probe and the control detection module are placed on the headband together. If the data is also transmitted by wire connection, it will be inconvenient to wear the device, so the short-range wireless transceiver function has become the best solution for wearable monitoring. A wireless transceiver module is added to the blood oxygen collection terminal, and the obtained human blood oxygen saturation value can be sent out wirelessly. In this way, the blood oxygen probe and the collection module can be placed together on the headband, and only a short wire connection is required between the two. The Bluetooth module JBM-141 is used in the design to form a Bluetooth module to achieve short-range wireless communication. When in use, the terminal is directly worn on the forehead of the human body, and the acquired data is sent to the handheld PDA through Bluetooth communication.

B. ANTI-MOTION INTERFERENCE WEARABLE DEVICE DESIGN

The wave group identification method based on template matching has a variety of specific implementation methods, including: 1). The maximum estimated variable threshold QRS wave detection method based on a priori, this method seeks a variety of probabilities based on prior knowledge Distribution, and calculate the maximum value of the joint probability, the calculation is very large; This method calculates the probability of sampling points corresponding to various states based on known sample values and states, and then combines the ECG signal to be processed with this probability distribution to identify QRS waves in the signal.

This method has certain discrimination for high P wave and high T wave.

If the acquisition module is the “body” of the sensor for sensing information, the system motherboard is the “brain” of the entire sensor. Not only does it need to implement a complete power management circuit, it also needs to provide control signals for the acquisition module, complete signal sampling and many functions such as wireless data transmission can be said that the system motherboard is the cornerstone of the entire sensor. For wearable sensors, the power consumption and volume requirements of the system board are more demanding. For wireless communication modules only, the power consumption of the commonly used classic Bluetooth or Zigbee protocol cannot meet the requirements of wearable continuous monitoring sensors, let alone other functional modules; in addition, due to the need for many functional modules, how to improve the system motherboard The degree of integration and the reduction in volume are also problems faced by wearable sensors.

For wearable devices, rechargeable battery management is still one of the better choices because the battery has higher storage energy density, lower self-discharge rate, no memory effect and more than other types of batteries. The advantages of high and low temperature adaptability are strong, so in this design, the battery is still used to power the sensor system. However, the battery is also “fragile”, improper charging and discharging operations will greatly affect the life of the battery, and thus affect the working life of the system, such as deep discharge will cause permanent damage to the battery, and the overvoltage during charging Current will also reduce battery life, which will affect the continuous working time of the sensor. Therefore, a suitable power management circuit is essential for the entire sensor system, and its configuration method is shown in Table 3.

TABLE 3. System charging input current limit configuration scheme.

EN2	EN1	Maximum input current
0	0	100mA; USB100 mode
0	1	500mA; USB500 mode
1	0	Set by configuring the size of the external resistor at the ILIM pin
1	1	Standby (USB suspend mode)

Motion artifacts are one of the main factors that limit the application of various wearable physiological sensors in daily life. Especially for PPG signals, the interference caused by motion artifacts is a huge aspect. During the detection process, motion Muscle activity will cause the propagation path of the signal detection beam to change; on the other hand, due to the strong absorption of light by venous blood, and movement will cause the volume of venous blood in the blood vessel to change, greatly affecting the state of light absorption, Thereby destroying the morphological characteristics of the collected PPG signal. The most annoying thing is that the frequency range of motion artifacts overlaps with the PPG signal, and has strong randomness and unpredictability.

Therefore, it is difficult to effectively eliminate motion only by relying on the blind signal processing method (single parameter method) the interference of artifacts.

The accelerometer is currently standard on many wearable devices. Therefore, acquiring the motion reference signal through the accelerometer can avoid the additional hardware cost of the system in future practical applications, so this topic attempts to use the motion sensor to obtain the reference signal; on the other hand, because The system cannot obtain a priori knowledge of the statistical characteristics of motion artifacts, so this topic uses an adaptive filter to automatically adjust the filter coefficients during the iterative process, thereby estimating and eliminating noise components in the expected signal. The overall algorithm architecture is shown in Figure 5.

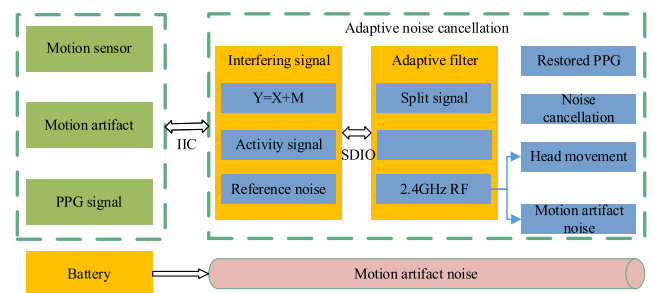


FIGURE 5. Anti-motion interference wearable device architecture.

In order to be able to provide accurate motion reference signals, it is necessary to provide as detailed motion information as possible. At the same time, an integrated high-precision ADC needs to be used to reduce quantization errors. Therefore, the MPU6050 motion sensor was selected in this topic, which not only integrates high-performance 3-axis the accelerometer has a measurement range of up to 16g. It also integrates a gyroscope and a 16-bit high-precision ADC. It can provide accurate motion information and is very suitable for anti-motion interference research. In addition, the built-in digital motion processor can directly output quaternions, reducing the workload of our MCU and avoiding cumbersome filtering and data fusion.

According to the nature of the above noise sources, measures can be taken through both hardware and software to reduce the level of noise interference. On the hardware, the general processing method is to design a hardware filter and a trap circuit, and realize the filtering at the hardware level through complex circuit design. This scheme has certain effects, but at the same time it will inevitably bring about problems such as increased system power consumption, complicated circuit structure and increased costs. This paper uses reasonable sensing the layout of the device, the design of the shielding structure and the setting of the guide rails of the wearable leads reduce the noise introduced by the lead wires from the perspective of the system structure. In software, the digital filtering method has also been well applied. The digital filter has high reliability and high accuracy because it

does not increase the hardware cost. MCUs commonly used in wearable devices are optimized for power consumption, with limited system resources and computing power (compared to FPGA and DSP), this brings certain difficulties to the design of software real-time filters.

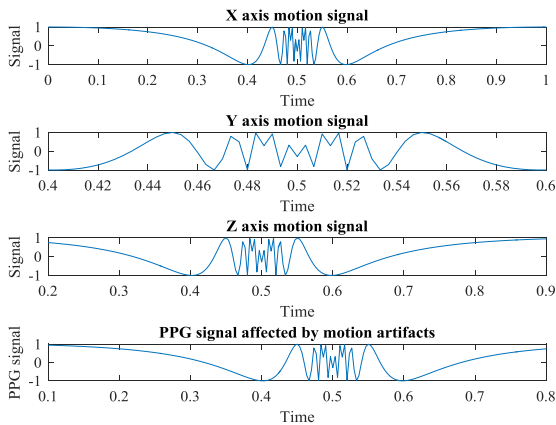


FIGURE 6. Synchronously collected 3-axis acceleration signal and PPG signal.

After the PSOC embedded programming is completed, the 3-axis acceleration signal and PPG signal can be obtained at the same time, as shown in Figure 6. It can be clearly seen from the figure that when there is no motion interference, the 3-axis acceleration signal tends to be stable, and the PPG signal shape remains intact; during the data collection, the motion signal acquisition module successfully captures the 3-axis acceleration signal. The PPG signal is also disturbed, losing its morphological characteristics; from the figure, it can be found that the 3-axis acceleration signal has a certain correlation with the motion artifacts in the PPG signal, and it also shows that the designed motion acquisition module functions normally and can be used for Research.

Because the motion noise encountered by the wearable PPG sensor in the actual application process is random and time-varying, it is impossible to obtain a priori knowledge of the statistical characteristics of the noise in advance. Relatively speaking, the adaptive filter can gradually estimate the required statistical characteristics during the operation, thereby tracking the statistical characteristics of the input signal, and automatically updating the filter weight coefficients to achieve the best filtering effect.

The adaptive filter interference cancellation model has two input signals: one is the actually collected PPG signal $y(k)$, which is the expected response of the adaptive filter and is generated by the motion artifacts caused by the superposition of pure PPG signals which is:

$$y(k) = s(k) + n(k) \quad (9)$$

The other input signal is the motion signal $m(k)$ obtained by the acceleration sensor, $O(k)$ is the output signal of the adaptive filter at time k , and the actual output signal of the adaptive interference cancellation model is the

error signal $e(k)$, So the output of the interference cancellation model is the difference between the desired response signal $y(k)$ and the filter output $O(k)$:

$$e(k) = y(k) - o(k) \quad (10)$$

The algorithm of the entire adaptive filter is as follows:

- (1) Any starting value is used as the filter weight coefficient vector at $k = 0$;
- (2) Calculate the error signal from the filter weight vector at time k , the input signal $m(k)$ and the expected response $y(k)$;
- (3) Use recursive method to update the filter weight coefficient vector
- (4) Increase the time parameter k by 1 and repeat steps (2) and (3) until the steady state is reached.

From the filtering results, the NLMS adaptive filter based on the motion reference signal has a certain suppression effect on the motion artifacts, and has great value for improving the stability of the wearable PPG sensor.

IV. EXPERIMENTS AND RESULTS

A. ANTI-INTERFERENCE ALGORITHM AND EXPERIMENTAL DATA ANALYSIS

In the design, the processor directly collects the frequency signal output by the receiving head, and does not process the analog signal. Therefore, the signal contains many interference to be eliminated, the main ones include background light noise, low blood perfusion, electrical interference, probe coupling interference and motion interference. In order to obtain an accurate blood oxygen saturation value, the collected original signal must be digitally processed.

First, the original PPG signal and interference are classified according to the spectral characteristics, which can be regarded as the superposition of the target signal and the interference signal:

$$P = S_{ac} + S_{dc} + N_{ac} + N_{de} \quad (11)$$

where S_{ac} , S_{dc} is the AC and DC components of the target signal, and N_{ac} , N_{de} represents the high frequency noise superimposed on the AC component, the low frequency noise superimposed on the DC component, and the noise of the frequency band and the PPG signal.

For low-frequency and high-frequency noise, it can be easily eliminated with digital filters. Collect a period of 2s of data and process it. Figure 7 shows the PPG signal before and after digital filtering. After digital filtering, high-frequency noise and low-frequency baseline drift are effectively eliminated, but the frequency aliased signal is still included.

For frequency aliasing interference, simple filtering cannot be eliminated, and this noise is usually introduced by motion interference. For wearable blood oxygen saturation monitoring, the removal of exercise interference is particularly important. Therefore, the design aims at this interference, and proposes an adaptive cancellation algorithm for blood oxygen saturation interference separation, which eliminates

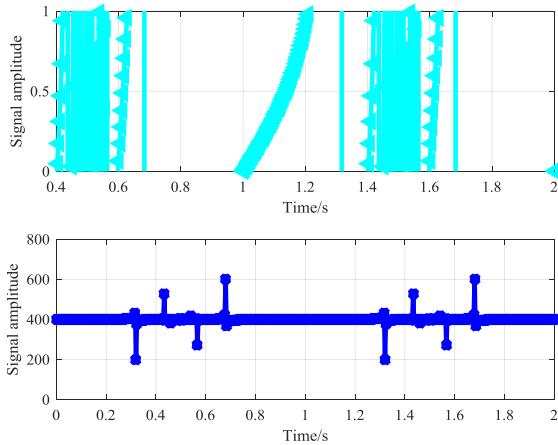


FIGURE 7. PPG signal before and after digital filtering.

the interference of motion on the calculation results from the AC component of the PPG signal.

The algorithm is based on an assumption: within a short period of time, the human blood oxygen saturation value is in a relatively constant state. When no motion interference is introduced, the PPG signal is relatively stable, and its AC component appears as a smooth signal; while when it is subjected to motion interference, the AC component of the PPG signal will fluctuate. If the AC component of the signal is calculated by the peak-to-peak value, the amount of data obtained will be too small, and it takes a long time for adaptive noise reduction to converge the output. Therefore, the method of calculating the signal envelope is used to expand the amount of data, so that the fluctuation trend of interference in the AC component of PPG can be better extracted.

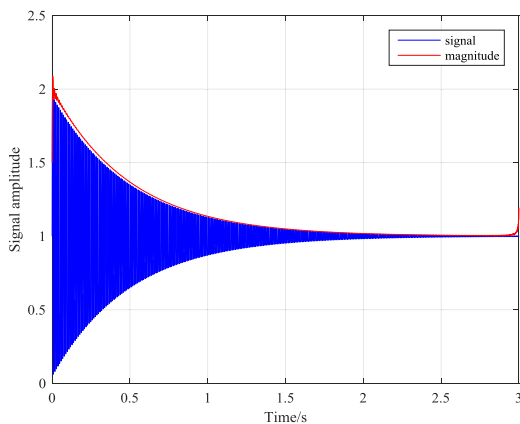
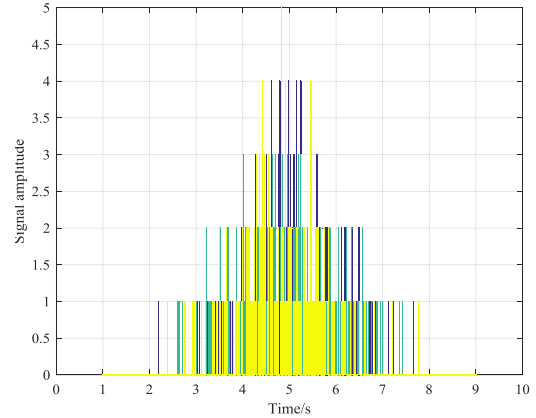
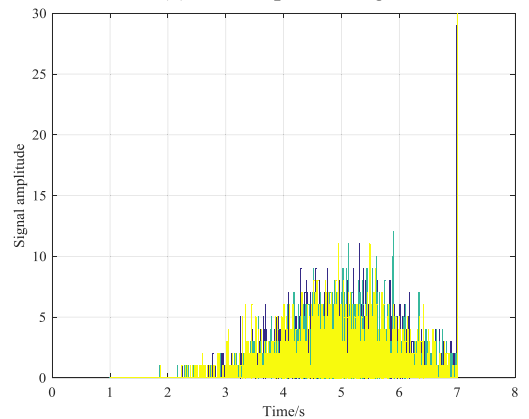


FIGURE 8. PPG signal upper and lower envelope.

As shown in Figure 8, the upper and lower envelopes of the signal are calculated and subtracted to obtain the AC component of the PPG signal. The red light PPG AC component r_{dac} and the infrared light PPG signal AC component i_{rac} are differentiated to obtain the difference Δac between the two. According to the assumption, PPG signal fluctuations are caused by motion, and ac contains the interference of motion on the signal, and its AC component is related to motion interference. Therefore, the AC component is extracted from



(a) Before processing



(b) After processing

FIGURE 9. AC components of two lights before and after adaptive noise reduction.

the difference signal as a reference signal, and the AC components of the two lights are adaptively denoised to obtain a clean signal.

$$\text{Red light PPG} = AC * i_{rac} + \Delta ac \quad (12)$$

Perform adaptive noise reduction on the collected 10 s signal. As shown in Figure 9, the AC components of the two optical PPG signals still fluctuate with motion after processing, but their fluctuations tend to be consistent. This is because before treatment, due to movement interference, the light path changes when passing through human tissues. Due to the different attenuation coefficients of deoxyhemoglobin and oxyhemoglobin for different wavelengths of light waves, the degree of fluctuation of the emitted light is different, as shown in Figure 9 The signal before processing is shown. After processing, the fluctuation difference of the two lights caused by the movement is eliminated, so the exchange ratio of the two lights tends to a stable value. Through the processed AC and DC components, an accurate blood oxygen saturation value can be calculated.

B. BLOOD OXYGEN SATURATOR MONITORING WITH SLIDING WINDOW ALGORITHM

In the experiment, when testing the performance of joint source channel coding and decoding based on the sliding

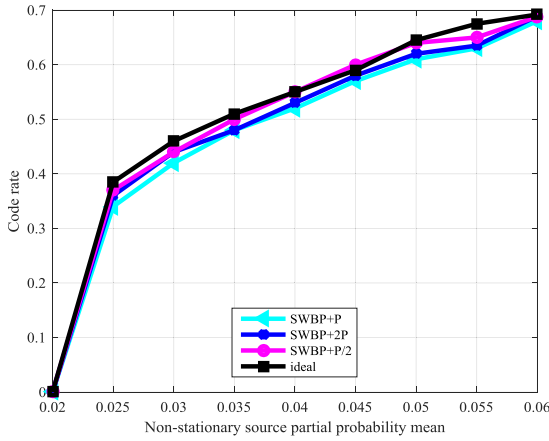
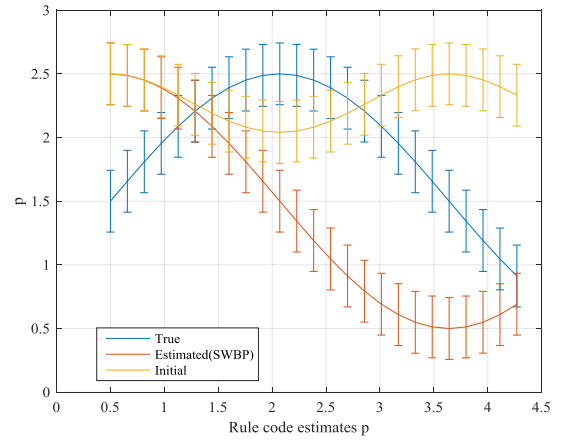


FIGURE 10. Regular LDPC codes when q is a fixed value.

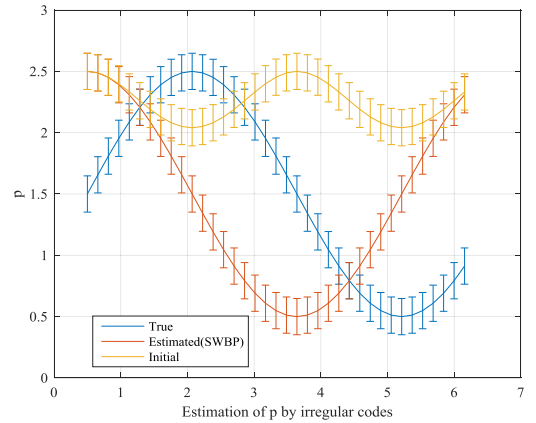
window confidence propagation algorithm, it is assumed that the channel parameters are known, and the non-stationary source statistical parameters P take values 0.02, 0.03, 0.04, 0.05, 0.06, 0.07, respectively. Fig. 10 shows the experimental effect of regular LDPC codes. static represents the code rate obtained by using the estimated value of the non-stationary source mean instead of the local partial probability; ideal represents the code rate that the algorithm can achieve under the premise of accurately knowing the local statistical characteristics of the non-stationary source; SWBP + 2P and SWBP+P/2 represent the code rate that the improved sliding window algorithm can compress the non-stationary source. The distribution uses the parameters p , $2p$ and $p / 2$ to initialize the confidence of the variable node; abscissa p represents the mean value of partial probability of non-stationary sources, and the ordinate represents the code rate.

From the analysis in Figure 10, we can see that the decoding performance of the algorithm is the worst in the static case, that is, the curve represented by static, because the parameters of the non-stationary source are not estimated, and the non-stationary source is treated as a stationary source. Ideally, the best performance, the ideal curve, is equivalent to knowing the statistical characteristics of non-stationary sources accurately at the decoding end. However, the statistical characteristics of non-stationary sources are often difficult to obtain. Columns SWBP+P, SWBP+2P, and SWBP+P/2 basically coincide with each other, and are very close to the ideal column, which means that after adding the parameter estimation algorithm, the code rate of the algorithm is close to the ideal situation, and the three curves are basically Coincidence means that the algorithm is robust to the initialization parameter p .

An important indicator for evaluating the performance of the parameter estimation algorithm is the difference between the estimated value and the accurate value, as shown in Figure 11. True in the figure represents the accurate value of the non-stationary source channel parameters, Estimated (SWBP) represents the estimated value of the improved sliding window confidence propagation algorithm, and Initial represents the initialization value of the algorithm,



(a) Estimation of p by regular LDPC codes



(b) Estimation of p for irregular LDPC codes

FIGURE 11. Experimental results of non-stationary parameter estimation.

that is, the mean value of the non-stationary source channel partial probability. Figures 11 (a) and 11 (b) show the effect of non-stationary source parameter estimation, where P takes a value of 0.07, the left figure represents the regular LDPC code, and the right figure represents the irregular LDPC code. It can be seen from the analysis in the figure that the improved sliding window confidence propagation algorithm estimates the local statistical characteristics of non-stationary sources and the local partial probability of non-stationary noise close to the true values. The statistical characteristics of the source channel used in this experiment follow a sine function. Since the sliding window confidence propagation algorithm estimates the local statistical characteristics of the current variable node depending on the confidence of its surrounding variable nodes, this method is also applicable to other continuous non-stationary sources.

In the stability test of the oximeter, if the state of the tester is basically unchanged and the phase of the input signal amplitude is unchanged, the upper and lower amplitude ranges of the experimental results measured by the homemade oximeter will reflect the homemade blood Oxygen stability.

The basic information of tester one: male, 26 years old, height 178mm, weight 67kg. Table 4 shows the measured experimental results and the calculated absolute error values.

TABLE 4. Results and absolute error of the first set of stability tests of the oximeter.

Serial number	Blood oxygen saturation		Pulse rate	
	SpO2	Absolute error	PR	Absolute error
1	96	0.4	79	0.18
2	98	0.57	79	0.2
3	95	0.62	77	0.81
4	94	0.43	76	0.23
5	95	0.4	76	0.22

Basic information of tester two: male, 24 years old, 182mm tall, 75kg weight. Table 5 shows the measured experimental results and the calculated absolute error values.

TABLE 5. Results and absolute error of the second group of oximeter stability experiment.

Serial number	Blood oxygen saturation		Pulse rate	
	SpO2	Absolute error	PR	Absolute error
1	98	0.21	74	0.41
2	98	0.23	74	0.42
3	98	0.2	74	0.43
4	96	0.23	75	0.67
5	97	0.82	75	0.62

The basic information of tester three: female, 25 years old, height 171mm, weight 57kg. Table 6 shows the measured experimental results and the calculated absolute error values.

TABLE 6. Results and absolute error of the first set of stability tests of the oximeter.

Serial number	Blood oxygen saturation		Pulse rate	
	SpO2	Absolute error	PR	Absolute error
1	97	0.62	69	0.62
2	98	0.43	68	0.43
3	99	0.67	68	0.42
4	96	0.42	67	0.6
5	95	0.41	67	0.42

From the three sets of blood oxygen saturation value SpO2 and pulse rate PR data monitored by this oximeter, the absolute error of each set of data is less than 1, so that the measured experimental data results are basically stable, which proves that The instrument has better stability.

Comparing the pulse wave signals of the three channels, the baseline drift of the red and green channels has the same trend. This baseline drift is first suppressed in the differential channel. The occurrence of this baseline drift has a certain correlation with the body's respiration. At the same time, the baseline drift in the red and green light channels is not completely consistent, which also reflects the change in blood oxygen concentration in the tissue. There is a certain difference in depth.

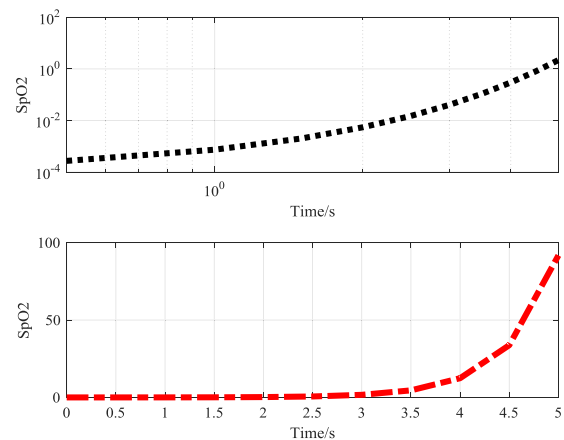
As shown in Table 7, differential channels are least affected by motion interference and have the strongest resistance to motion interference. The AR value of the green light channel is smaller than that of the red light channel in the four motion modes, indicating that the green light channel itself has

TABLE 7. Statistics of noise ratio during different movements.

Aisle	Exercise one	Exercise two
Red light channel	1.53	8.65
Green light channel	1.28	5.93
Differential channel	1.26	1.45

stronger anti-interference ability than the red light channel. Easily is affected by deep tissue movement. Among the four motion modes in the experiment, the signal-to-noise ratio of Motion 2 is the most obvious. In Motion 2, the AR of the red channel is 8.65, the AR of the green channel is 5.93, and the AR of the differential channel is 1.45.

Collect a period of 10 s and 98% normal blood oxygen saturation data with strong motion interference for calculation. The calculation results are shown in Figure 12.

**FIGURE 12. Calculation results when the blood oxygen saturation value is 98%.**

Calculated by traditional methods, each pulse wave can only get one result. When it is affected by movement interference, there is a calculation deviation, and the result is lower than 98% of the normal blood oxygen saturation value; and the adaptive cancellation algorithm is used to calculate the obtained error is less than 1%, which is close to the true value. The experimental results in this paper prove the rationality of the designed model, and verify that the method of using red light channel, green light channel and differential channel to simultaneously collect pulse wave signals to improve the system's ability to resist motion interference is feasible and can improve signal noise ratio.

V. CONCLUSION

The sliding window confidence propagation algorithm can be used to estimate the parameters of non-stationary sources and reduce the compression rate of non-stationary sources. In this paper, based on the sliding window confidence propagation algorithm, by analyzing the characteristics of the algorithm, the weights of variable nodes in the sliding window are assigned. For different non-stationary sources, a unified model is established, and different loss functions

are used to make the estimation more accurate. Analyze the reasons that affect the time performance of the sliding window confidence propagation algorithm. By adding correlation coefficients to skip some inefficient iterative estimation links, the time performance of the algorithm is improved by more than 1.5 times. By analyzing the correlation between non-stationary source compression and channel coding, an improved sliding window confidence propagation algorithm is used to estimate the non-stationary channel noise. Using two different LDPC codes to test the decoding performance of the improved algorithm, the experimental results show that the algorithm can achieve the ideal decoding performance with the channel noise parameters known at the decoding end. Starting from the three aspects of structure, power consumption and interference, a wearable blood oxygen saturation monitoring terminal is designed to realize the miniaturization of the device and ensure its wearability; at the same time, the LED lighting and the processor are controlled through intermittent timing Working time saves energy consumption of equipment and prolongs working time. In terms of motion interference, an envelope adaptive algorithm for the calculation of blood oxygen saturation is adopted. Through the processing and analysis of experimental data, the effectiveness of the algorithm is confirmed. The design integrates the probe and acquisition module in the headband, and adds wireless communication functions to form a wearable blood oxygen monitor. In the future research and development, it can be used as a terminal node of the wearable multi-physiological parameter real-time monitoring system to join the wireless body area network, which has very good application prospects.

REFERENCES

- [1] J. Yan and G. Bin, "Research on an anti-motion interference algorithm of blood oxygen saturation based on AC and DC analysis," *Technol. Health Care Off. J. Eur. Soc. Eng. Med.*, vol. 23, no. 2, pp. S285–S291, 2015.
- [2] R. F. Keefe, E. G. Zimelman, and A. M. Wempe, "Use of smartphone sensors to quantify the productive cycle elements of hand fallers on industrial cable logging operations," *Int. J. Forest Eng.*, vol. 30, no. 2, pp. 132–143, May 2019.
- [3] M. Gochoo, T.-H. Tan, S.-H. Liu, F.-R. Jean, F. S. Alnajjar, and S.-C. Huang, "Unobtrusive activity recognition of elderly people living alone using anonymous binary sensors and DCNN," *IEEE J. Biomed. Health Inform.*, vol. 23, no. 2, pp. 693–702, Mar. 2019.
- [4] M. Mangiarotti, F. Ferrise, S. Graziosi, F. Tamburrino, and M. Bordegoni, "A wearable device to detect in real-time bimanual gestures of basketball players during training sessions," *J. Comput. Inf. Sci. Eng.*, vol. 19, no. 1, pp. 11004.1–011004.10, Mar. 2019.
- [5] C. A. Majmudar and B. I. Morshed, "Autonomous OA removal in real-time from single channel EEG data on a wearable device using a hybrid algebraic-wavelet algorithm," *ACM Trans. Embedded Comput. Syst.*, vol. 16, no. 1, pp. 1–16, Nov. 2016.
- [6] K. B. Narayanan and H. H. Park, "Toll/interleukin-1 receptor (TIR) domain-mediated cellular signaling pathways," *Apoptosis*, vol. 20, no. 2, pp. 196–209, Feb. 2015.
- [7] C. Zhou, C. Tu, J. Tian, J. Feng, Y. Gao, and X. Ye, "A low power miniaturized monitoring system of six human physiological parameters based on wearable body sensor network," *Sensor Rev.*, vol. 35, no. 2, pp. 210–218, Mar. 2015.
- [8] L. Li, X. Wang, and K. Lu, "Near-infrared spectra noninvasive measurement method of blood oxygen saturation based on the 'M+ N' theory," *Shengwu Yixue Gongchengxue Zazhi*, vol. 33, no. 5, pp. 885–889, 2016.
- [9] Y. Li, N. Yang, L. Li, L. Liu, and Y. Yang, "Finger gesture recognition using a smartwatch with integrated motion sensors," *Web Intell. Agent Syst.*, vol. 16, no. 2, pp. 123–129, Jun. 2018.
- [10] F. Santoso and S. J. Redmond, "Indoor location-aware medical systems for smart homecare and telehealth monitoring: State-of-the-art," *Physiol. Meas.*, vol. 36, no. 10, pp. R53–R87, Oct. 2015.
- [11] Y. Togashi, J. Shirakawa, T. Okuyama, S. Yamazaki, M. Kyohara, A. Miyazawa, T. Suzuki, M. Hamada, and Y. Terauchi, "Evaluation of the appropriateness of using glucometers for measuring the blood glucose levels in mice," *Sci. Rep.*, vol. 6, no. 1, pp. 25465–25473, May 2016.
- [12] G.-D. Liu, Z.-Y. Cao, G. Zhou, X.-Y. Zhou, J. Cai, Y.-T. Zha, and C.-H. Qian, "A anti-disturbance cerebral oxygen analyzer based on near-infrared spectra," *Opt. Precis. Eng.*, vol. 24, no. 8, pp. 1846–1853, 2016.
- [13] W. Pei, H. Zhang, Y. Wang, X. Guo, X. Xing, Y. Huang, Y. Xie, X. Yang, and H. Chen, "Skin-potential variation insensitive dry electrodes for ECG recording," *IEEE Trans. Biomed. Eng.*, vol. 64, no. 2, pp. 463–470, Feb. 2017.
- [14] J. Lu, X. Zhang, and H. Xiong, "A new method for suppressing periodic narrowband interference based on the chaotic van der Pol oscillator," *Int. J. Bifurcation Chaos*, vol. 25, no. 9, pp. 120–155, 2015.
- [15] J. Wang, Y. Han, L. M. Wang, P. Z. Zhang, and P. Chen, "Instantaneous frequency estimation for motion echo signal of projectile in bore based on polynomial chirplet transform," *Russian J. Nondestruct. Test.*, vol. 54, no. 1, pp. 44–54, Jan. 2018.
- [16] Y.-N. Yu, F. Doctor, S.-Z. Fan, and J.-S. Shieh, "An adaptive monitoring scheme for automatic control of anaesthesia in dynamic surgical environments based on bispectral index and blood pressure," *J. Med. Syst.*, vol. 42, no. 5, pp. 95–106, May 2018.
- [17] F. Fan, Y. Yan, Y. Tang, and H. Zhang, "A motion-tolerant approach for monitoring SpO₂ and heart rate using photoplethysmography signal with dual frame length processing and multi-classifier fusion," *Comput. Biol. Med.*, vol. 91, pp. 291–305, Dec. 2017.
- [18] W. Liao, J. Shi, and J. Wang, "Electromagnetic interference of wireless power transfer system on wearable electrocardiogram," *IET Microw., Antennas Propag.*, vol. 11, no. 3, pp. 330–335, Feb. 2017.
- [19] Q. Guan, "Multi user interference cancellation in satellite to ground uplink system based on improved WPIC algorithm," *KSI Trans. Internet Inf. Syst.*, vol. 10, no. 11, pp. 5497–5512, 2016.
- [20] B. Yang, Y. Yang, J. Yang, and Z. Guo, "SINS anti-interrupt self-alignment algorithm for angular swaying and linear motion coupling interference," *Chin. J. Sens. Actuators*, vol. 28, no. 4, pp. 526–530, 2016.
- [21] J. C. González-Olvera, J. Martínez-Reyes, and E. González-Jasso, "Determination of pKa values for deprotonable nucleobases in short model oligonucleotides FRET-based nanobiosensors for imaging intracellular," *Drilling Prod. Technol.*, vol. 156, no. 6, pp. 1622–1634, 2015.
- [22] D. B. Bollini, M. M. Naidu, and M. R. Nuka, "Measurement of mobile switching centres throughput in GSM network integrating sliding window algorithm with a single server finite queuing model," *J. Comput. Netw. Commun.*, vol. 2016, pp. 1–10, Oct. 2016.
- [23] W. Song, R. Zhang, Y. Yao, Y. Liu, and Y. Hu, "PPP sliding window algorithm and its application in deformation monitoring," *Sci. Rep.*, vol. 6, no. 1, pp. 26497–26504, Sep. 2016.
- [24] R. Carmona-Cabezas, J. Gómez-Gómez, E. G. de Ravé, and F. J. Jiménez-Hornero, "A sliding window-based algorithm for faster transformation of time series into complex networks," *Chaos*, vol. 29, no. 10, pp. 103121–103129, 2019.
- [25] M. de-Frutos-López, J. L. González-de-Suso, S. Sanz-Rodríguez, C. Peláez-Moreno, and F. Díaz-de-María, "Two-level sliding-window VBR control algorithm for video on demand streaming," *Signal Process., Image Commun.*, vol. 36, pp. 1–13, Aug. 2015.
- [26] S. K. Jain, "Algorithm for dealing with time-varying signal within sliding-window for harmonics estimation," *IET Sci. Meas. Technol.*, vol. 9, no. 8, pp. 1023–1031, 2015.
- [27] C. Chen, Y. Xiang, Y. DengLiu, and Z. Zhou, "Research on cache timing attack against RSA with sliding window exponentiation algorithm," *Int. J. Interdiscipl. Telecommun. Netw.*, vol. 8, no. 2, pp. 88–95, Apr. 2016.
- [28] M. M. Found, M. G. Mostafa, A. S. Mashat, and T. F. Gharib, "WSWF: A weighted sliding window filtering algorithm for frequent weighted itemsets mining," *Int. J. Innov. Comput., Inf. Control*, vol. 11, no. 4, pp. 1421–1439, 2016.
- [29] D. Wei and Z. Xianxia, "Research on sliding window join semantics and join algorithm in heterogeneous data streams," *Open Cybern. Systemics J.*, vol. 9, no. 1, pp. 556–564, Jun. 2015.

- [30] Q. Liu, K. Wang, and W. Rao, "Non-equal time series clustering algorithm with sliding window STS distance," *J. Frontiers Comput. Sci. Technol.*, vol. 9, no. 11, pp. 1301–1313, 2015.
- [31] I. Chakroun, T. Haber, and T. J. Ashby, "SW-SGD: The sliding window stochastic gradient descent algorithm," *Procedia Comput. Sci.*, vol. 108, no. C, pp. 2318–2322, 2017.
- [32] C. Bo, D. C. Yong, and G. Xiue, "A frequent pattern parallel mining algorithm based on distributed sliding window," *Int. J. Comput. Syst. Sci. Eng.*, vol. 31, no. 2, pp. 101–107, 2016.
- [33] L. Huimin, D. Tianyi, S. Jingjing, S. Hongyang, H. Xuming, and L. Gang, "Translation registration algorithm for multi-source time series data based on the sliding window," *J. Eng. Sci. Technol. Rev.*, vol. 9, no. 5, pp. 44–50, 2016.
- [34] Z. Sun, Z. He, and T. Zang, "Estimating fundamental parameters by using sliding-window spectrum separation algorithm," *Zhongguo Dianji Gongcheng Xuebao*, vol. 37, no. 19, pp. 5604–5612, 2017.
- [35] B. Shan and Y. Fang, "GPU accelerated parallel algorithm of sliding-window belief propagation for LDPC codes," *Int. J. Parallel Program.*, vol. 48, no. 3, pp. 566–579, Jun. 2020.
- [36] S. Jain and R. K. Bansal, "On match lengths, zero entropy, and large deviations—With application to sliding window Lempel–Ziv algorithm," *IEEE Trans. Inf. Theory*, vol. 61, no. 1, pp. 120–132, Jan. 2015.
- [37] S. Lai, L. Wan, and X. Zeng, "Comparative study of sliding window multifractal detrended fluctuation analysis and multifractal moving average algorithm," *J. Phys. Conf. Ser.*, vol. 1345, no. 4, pp. 42086–42093, 2019.
- [38] Z. Li and T. Ran, "Application of a sliding-window data accumulation algorithm for improving security in radiant intensity detection systems," *J. Univ. Sci. Technol. China*, vol. 45, no. 1, pp. 56–60, 2015.



BIN JIAO was born in Henan, China, in 1978. He received the bachelor's degree from the Northwestern Institute of Light Industry, in 2002, and the master's degree from Jiangnan University, in 2010. Since 2002, he has been working with the Zhengzhou University of Aeronautics. He has published 30 articles, eight of which have been included by EI. His research interests include product design and wearable devices.

• • •